Special issue: ICAMSF2025

Institution of MECHANICAL ENGINEERS
Journal of ENGINEERING TRIBOLOGY

Proc IMechE Part J:
J Engineering Tribology
1–17

DOI: 10.1177/13506501251372828
journals.sagepub.com/home/pij
Sage

# Wear performance and optimization of h-BN-modified AZ91/$TiB_2$ magnesium composites under dry sliding conditions

**Sathish Kamaraj[1], Baskar Sanjeevi[1], Hariharasakthisudhan Ponnarengan[2], Logesh Kamaraj[3] and Sathickbasha Katharbasha[4]**

## Abstract

This study investigates the dry sliding tribological behavior of AZ91 magnesium alloy reinforced with titanium diboride ($TiB_2$) and hexagonal boron nitride (h-BN) ceramic particles. The primary objective was to enhance wear resistance and reduce the coefficient of friction (COF) through a synergistic reinforcement approach. Hybrid composites were fabricated using a two-stage stir casting process integrating mechanical and ultrasonic agitation to ensure uniform dispersion of the reinforcements. Experiments were conducted using a Taguchi L16 orthogonal array, and the influence of normal load, sliding speed, h-BN content, and sliding distance on wear and COF was evaluated under ASTM G99 conditions. Signal-to-noise ratio analysis revealed that normal load and h-BN content were the most significant factors influencing wear rate and COF, respectively. Gradient Boosting Regression (GBR) models were developed to predict the responses, achieving $R^2$ values of 0.816 for wear rate and 0.825 for COF. The GBR models were then integrated with a Multi-Objective Particle Swarm Optimization (MOPSO) algorithm to identify Pareto-optimal conditions. The optimum solution (Normal load = 40 N, Speed = 1.0076 m/s, h-BN = 1.1731wt.%, Distance = 1 km) yielded wear rate and COF values of 14.98 mg/km and 0.2517, with <4% deviation from predictions. SEM analysis of worn surfaces confirmed mechanisms including micro grooving, tribolayer formation, and debris-controlled wear. The GBR–MOPSO hybrid framework proved effective for optimizing and understanding the complex wear-friction interplay in AZ91 hybrid composites.

## Keywords

AZ91 magnesium alloy, hybrid composites, tribology, gradient boosting regression, multi-objective optimization

Received: 29 April 2025; accepted: 12 August 2025

## Introduction

Lightweight structural materials with enhanced surface durability are increasingly sought after in the automotive, aerospace, and industrial sectors, where frictional and wear losses significantly impact system reliability and energy efficiency. Among these materials, magnesium alloys, particularly AZ91 (Mg–9Al–1Zn), have emerged as promising candidates owing to their exceptional specific strength-to-weight ratios, favorable castability, and moderate corrosion resistance.[1,2] Nevertheless, the intrinsic limitations of AZ91, namely its low hardness, high chemical reactivity, and insufficient wear resistance under dry sliding conditions, significantly hinder its broader deployment in demanding tribological environments.

In response to these challenges, extensive research has been conducted on the hybridization of magnesium alloy-based composites to tailor and enhance their mechanical and tribological properties. Mohammed Fahad et al. demonstrated that the hybrid reinforcement of AZ91D magnesium alloy with WC and $SiO_2$ particles markedly improved both wear resistance and hardness, rendering it more suitable for aviation applications.[3] Building upon such strategies, Prem Sagar et al. revealed that hybridizing AZ31B magnesium alloy with fly ash and nano-TiC through friction stir processing resulted in a twentyfold reduction in grain size, a 1.72-fold increase in microhardness, a 2.42-fold improvement in tensile strength, a 2.57-fold increase in compressive strength, and approximately an 80% enhancement in wear resistance over the base alloy.[4]

Continuing on the trajectory of hybridization approaches, V. Preethi et al. found that integrating 0.3% graphene oxide and up to 15% $Si_3N_4$ into magnesium alloys substantially reduced the wear rate to $0.9197 \times 10^{-3}$ $mm^3/Nm$ and the

[1]Department of Mechanical Engineering, Vels Institute of Science Technology and Advanced Studies, Chennai, Tamil Nadu, India
[2]Department of Mechanical Engineering, Dr Mahalingam College of Engineering and Technology, Pollachi, Tamil Nadu, India
[3]Department of Mechanical Engineering, Vel Tech Rangarajan Dr Sagunthala R&D Institute of Science and Technology, Chennai, Tamil Nadu, India
[4]Department of Mechanical Engineering, B.S. Abdur Rahman Crescent Institute of Science and Technology, Chennai, Tamil Nadu, India

**Corresponding author:**
Hariharasakthisudhan Ponnarengan, Department of Mechanical Engineering, Dr Mahalingam College of Engineering and Technology, Pollachi - 642 003, Tamil Nadu, India.
Email: harimeed2012@gmail.com

coefficient of friction (COF) to 0.4019 under optimal sliding conditions of 10 N load, 1 m/s velocity, and 1000 m sliding distance.[5] Similarly, KT Sunu Surendran et al. enhanced the tribological properties of a 6061 aluminium alloy matrix by hybridizing it with $B_4C$ and carbon nanotubes (CNT) using ultrasonic-assisted stir casting, which led to a hardness increase up to 109 VHN and superior self-lubricating performance with 10 vol.% CNT composites.[6] In parallel, Shoufa Liu et al. refined the grain size of AZ31B magnesium alloy from 7.39 μm to 3.38 μm by hybridizing with $CeO_2$ and $ZrO_2$ via friction stir processing, which concomitantly elevated the hardness, shear punching strength, tensile strength, and wear and corrosion resistance.[7]

As research advanced, newer hybrid systems and methods emerged to further improve magnesium alloys' performance. Gurmeet Singh Arora et al. utilized powder metallurgy to hybridize AZ31 magnesium alloy with $TiO_2$ and HAp, achieving higher compressive strength, improved microhardness, enhanced biocompatibility, and reduced wear loss.[8] Gnanasambandam Anbuchezhiyan et al. enhanced the mechanical properties of Mg–Al–Zn alloys by incorporating 9 wt % $B_4C$ and 3 wt% BN through stir casting, which improved tensile and compressive strengths, yield strength, hardness, and corrosion resistance.[9] Additionally, C. R. Mahesha et al. examined AZ60A magnesium alloy hybridized with boron nitride and graphite, noting significant improvements in wear rates under dry sliding conditions as determined through Taguchi analysis.[10]

To deepen understanding of wear optimization, several researchers applied machine learning (ML) models. Dhanunjay Kumar Ammisetti et al. used decision tree, random forest, and gradient boosting regression (GBR) models to predict the wear rate and COF of AZ91/Gr/$Al_2O_3$ composites, with the GBR model achieving an excellent $R^2$ of 98.89%.[11] In subsequent work, they showed that polynomial regression models could effectively predict the wear behavior of AZ31/$B_4C$/GNP composites.[12] Moreover, Surja Deka et al. employed feedforward and LSTM neural networks to model the wear and corrosion behavior of Mg/$CeO_2$ nanocomposites, confirming superior performance over monolithic magnesium.[13]

Expanding into bio-composite applications, Vijay Kumar Mahakur et al. applied ML models to predict wear in silane-treated jute–epoxy composites, with the support vector machine (SVM) model yielding the highest accuracy.[14] G. V. Jagadeesh et al. employed artificial neural networks (ANN) to model tribological properties of ball-burnished Mg Ze41A alloy, eely confirming notable improvements in wear resistance and friction reduction.[15] Similarly, Khursheed Ahmad Sheikh et al. demonstrated that random forest models outperformed SVR models in predicting wear behavior of ZA37 composites, highlighting the beneficial effects of SiC reinforcement and graphite-blended oil under lubricated conditions.[16]

Further investigations by Zhihong Zhu et al. confirmed that machine learning regression models could accurately predict tensile strength in SiC-reinforced magnesium matrix composites, establishing key processing parameters.[17] Other efforts, such as those by Khursheed Ahmad Sheikh et al., emphasized ML's predictive power for abrasive wear behavior in in-situ TiC-reinforced composites.[18]

Optimization techniques were also integrated with experimental designs to fine-tune wear and corrosion behaviors. Beniyel M et al. optimized AZ91D magnesium alloy wear parameters using response surface methodology (RSM) combined with a genetic algorithm (GA), achieving good experimental alignment.[19] Samuel Kefyalew Abebe et al. refined AZ61/SiC/$ZrO_2$ hybrid composites using a Box–Behnken RSM design and GA to minimize wear rate and maximize thermal stability.[20] Vignesh Packkirisamy et al. further validated RSM-GA optimization approaches for AZ31/5% YSZ composites.[21] Additional studies, such as those by T. Satish Kumar et al. on AZ31/TiC composites,[22] V. Raviteja Behera et al. on ZA27/SiC/$TiB_2$ composites,[23] and Kothuri Chenchu Kishor Kumar et al. on AZ31-SiC composites using the Whale Optimization Algorithm (WOA),[24] underscore the successful application of advanced optimization methodologies to achieve superior tribological properties.

Recent years have seen an accelerated integration of machine learning (ML) methodologies for optimizing the tribological and mechanical behavior of magnesium-based composites, underscoring the relevance and sophistication of data-driven approaches in materials engineering. Barun Haldar et al. demonstrated that Gradient Boosting Machine (GBM) models can accurately predict wear loss and friction coefficients in magnesium hybrid composites, identifying graphite content as the dominant parameter governing tribological performance under dry sliding conditions.[25] Similarly, Guosong Zhu et al. employed twelve ML algorithms to optimize the mechanical properties of magnesium alloys, where Gradient Boosting Regression (GBR) achieved approximately 89% predictive accuracy, facilitating inverse alloy design through solubility constraints and A-SMOTE oversampling techniques.[26] Dhanunjay Kumar Ammisetti et al. reported GBR models achieving $R^2$ values up to 98.89% for predicting wear rates in AZ91 magnesium composites reinforced with $Al_2O_3$ and graphene, revealing critical wear mechanisms such as delamination and abrasion under variable normal loads and sliding speeds.[27] Turan Gurgenc et al. utilized Extreme Learning Machine (ELM) to predict wear loss in AZ91D magnesium alloys treated via plasma and HVOF coatings, attaining $R^2 = 0.9901$, thereby illustrating the efficacy of ML in optimizing surface engineering processes.[28] Mahammod Babar Pasha et al. integrated ML models with experimental analyses to predict wear rate and friction behavior in Mg/$Si_3N_4$ nanocomposites, highlighting the role of uniform nanoparticle dispersion and robust interfacial bonding in enhancing wear resistance and lowering friction.[29] Reham Fathi et al. leveraged LightGBM algorithms to forecast wear behavior in functionally graded magnesium composites synthesized from recycled waste chips and eggshells, reporting localized improvements in hardness and wear resistance between inner and outer composite zones.[30] Furthermore, Akshansh Mishra et al. coupled Particle Swarm Optimization with GBR (PSO–GBR) to model AZ31 magnesium alloy wear rates under diverse sliding conditions, achieving remarkable predictive fidelity with $R^2 = 0.99970$, thus outperforming alternative PSO–Decision Tree models and effectively capturing nonlinear wear phenomena.[31] These studies underscore the expanding frontier of ML-driven optimization in magnesium and hybrid composites, not only enhancing predictive

**Table 1.** Composition of AZ91 alloy.

| Element | Mg | Al | Zn | Mn | Si | Cu | Ni | Fe |
|---|---|---|---|---|---|---|---|---|
| Wt.% | 89.758 | 9 | 0.8 | 0.3 | 0.08 | 0.03 | 0.017 | 0.015 |

accuracy for wear and mechanical responses but also enabling inverse design of compositions and process parameters. The present investigation builds upon this emerging paradigm by integrating GBR with Multi-Objective Particle Swarm Optimization (MOPSO), uniquely applying this hybrid modeling framework to optimize the dry sliding tribological performance of AZ91/$TiB_2$–h-BN composites and validate predictions through detailed SEM analysis of wear mechanisms.

Despite extensive efforts to enhance the wear and mechanical properties of AZ91 and related magnesium alloys through hybrid reinforcements and machine learning-based predictions, there remains a lack of integrated approaches combining optimized reinforcement selection, advanced predictive modeling, and real-time validation under diverse tribological conditions. The present research addresses this gap by developing a novel hybrid AZ91-based composite system optimized via machine learning and validated experimentally. The research objectives are to design hybrid composites with superior wear resistance, develop predictive ML models for wear behavior, and establish experimental validation strategies under varying operational conditions.

The parameters optimized in this study were selected for their decisive roles in the tribological response of AZ91-based composites under dry sliding. Normal load governs Hertzian stresses and plastic deformation, directly affecting subsurface damage and reinforcement stability. Sliding speed influences interfacial heat generation and the kinetics of tribo-film formation, where excessive velocities can trigger thermal softening and oxidative wear. The h-BN content, as a solid lubricant, reduces interfacial shear and friction but requires careful balancing to prevent agglomeration or reduced load transfer capacity. Sliding distance captures the evolution from transient wear to steady-state regimes, reflecting cumulative mechanical and thermal effects that shape tribolayer stability, oxidative debris formation, and fatigue crack initiation. Integrating these variables into a unified optimization framework ensures the simultaneous tailoring of material composition and operational parameters, enabling the development of AZ91/$TiB_2$–h-BN composites with minimized wear and friction while preserving mechanical integrity for advanced engineering applications.

## Materials and methods

In this investigation, AZ91 magnesium alloy was employed as the matrix material. The AZ91 alloy, procured from local vendors in Chennai, India, possessed a nominal chemical composition as detailed in Table 1, comprising magnesium (89.758 wt.%), aluminum (9 wt.%), zinc (0.8 wt.%), and minor constituents such as manganese, silicon, copper, nickel, and iron.

To enhance the mechanical robustness and tribological performance, titanium diboride ($TiB_2$) and hexagonal boron nitride (h-BN) ceramic reinforcements, each with a purity of 99.9%, were sourced from Sigma-Aldrich. Morphological characterization through scanning electron microscopy (SEM) revealed that $TiB_2$ particles exhibited angular and blocky geometries with an average particle size in the range of 5–8 μm as shown in Figure 1(a), while h-BN particles displayed a distinct morphology consisting of thin, stacked flake-like structures as represented in Figure 1(c). The elemental composition of the reinforcements was confirmed through energy-dispersive X-ray spectroscopy (EDS) analysis as displayed in Figures 1(b) and 1(d). The EDS results indicated that Ti and B elements constituted 94.08% and 5.92% of the $TiB_2$ reinforcement, respectively, whereas h-BN contained 63.37% nitrogen and 30.84% boron, along with minor traces of oxygen and other elements. The selection of $TiB_2$ and h-BN as dual reinforcements aimed to synergistically improve the wear resistance and coefficient of friction characteristics of the AZ91-based composites under dry sliding environments.

### Composite fabrication

The hybrid AZ91-based composites reinforced with $TiB_2$ and h-BN ceramic particles were fabricated using a two-stage stir casting route integrating both mechanical and ultrasonic agitation to ensure uniform dispersion of reinforcements. Initially, AZ91 alloy ingots were charged into a graphite crucible and melted at $750 \pm 5$ °C under a protective argon gas atmosphere to minimize oxidation. Simultaneously, $TiB_2$ and h-BN powders were preheated at 300 °C for 1 h to eliminate moisture and improve wettability. The amount of $TiB_2$ was maintained as 4 wt.%, which was identified as optimum percentage from the pilot study. The h-BN particles were added according to the experimental plan. Mechanical stirring was initiated at 500 rpm for 10 min using a four-blade impeller positioned at one-third depth of the melt to create a strong vortex. The preheated reinforcements were gradually introduced into the vortex, followed by continued stirring for an additional 10 min. Subsequently, ultrasonic treatment was applied at a frequency of 20 kHz and power of 1 kW for 5 min using a ceramic-coated titanium sonotrode, immersed directly into the melt to promote de-agglomeration and interfacial bonding. The homogenized slurry was then poured into a preheated steel mold (300 °C) and allowed to solidify under ambient conditions. This hybrid agitation technique was adopted to overcome the interfacial tension between ceramic reinforcements and the molten AZ91 matrix, thereby enhancing microstructural homogeneity and particle-matrix interfacial integrity.

In the present investigation, no post-casting heat treatment was applied to the AZ91/$TiB_2$–h-BN hybrid composites. This decision was deliberate, as the primary objective of this work was to evaluate the dry sliding tribological performance of the composites in their as-cast condition, capturing the intrinsic microstructural characteristics imparted by the combined mechanical and ultrasonic stirring process. Heat treatments, such as solutionizing and ageing, are often employed in magnesium alloys like AZ91 to dissolve the β-$Mg_{17}Al_{12}$ intermetallic phase and refine the microstructure, typically conducted at temperatures around 400–420 °C for solution treatment followed by ageing at approximately

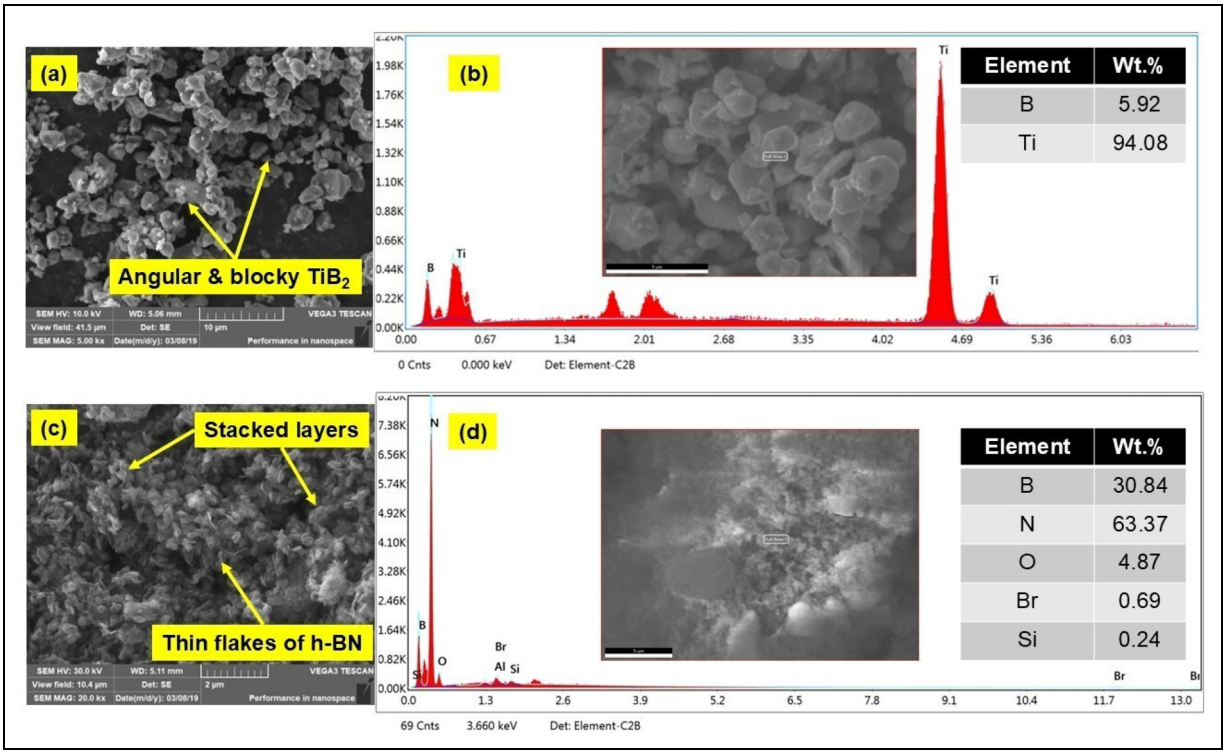


**Figure 1.** SEM and EDS analyses of reinforcements used in AZ91 composites: (a) $TiB_2$ particles with angular shape (5–8 μm), (b) EDS confirming Ti and B in $TiB_2$, (c) h-BN flakes with lamellar structure, and (d) EDS indicating B and N in h-BN

150–200 °C to precipitate fine β-phase particles. However, introducing such thermal cycles can result in complex effects in particle-reinforced composites. In particular, elevated temperatures could induce differential thermal expansion between the AZ91 matrix and the ceramic reinforcements, potentially generating residual stresses at the matrix–particle interfaces and risking interfacial decohesion, especially considering the significant thermal expansion mismatch between AZ91 ($\sim 26 \times 10^{-6}\,K^{-1}$) and $TiB_2$ ($\sim 7.5 \times 10^{-6}\,K^{-1}$). Furthermore, the lamellar structure of h-BN, which is crucial for its solid lubrication behavior, might undergo morphological alterations or partial oxidation during heat treatment, diminishing its capacity to reduce interfacial shear stress and maintain a low coefficient of friction. Additionally, prolonged thermal exposure could promote grain coarsening in the AZ91 matrix and excessive growth of intermetallic phases, which may negatively affect the load-bearing capability provided by the finely dispersed $TiB_2$ particles and compromise the uniformity achieved during casting. Therefore, to maintain the microstructural integrity and ensure that the observed tribological responses directly reflected the effects of hybrid reinforcement and processing methods, the composites were retained in the as-cast state for all experimental evaluations. This approach enabled a focused assessment of the synergistic interaction between $TiB_2$'s load-bearing reinforcement and h-BN's solid lubrication role under dry sliding conditions, without introducing additional variables associated with thermal post-processing.

High-resolution SEM examination revealed critical microstructural features of the AZ91/$TiB_2$–h-BN hybrid composites, confirming the effectiveness of the fabrication process. As shown in Figure 2(a), a uniform distribution of reinforcement particles is evident under bright-field imaging at 100× magnification, indicating successful dispersion achieved through combined mechanical and ultrasonic stirring. The continuous AZ91 Mg matrix, visible in Figure 2(b) at 250×, is free from major agglomerations, ensuring consistent load transfer during sliding wear conditions. At 500× magnification, Figure 2(c) demonstrates clean interfaces between reinforcement particles and the matrix, along with well-defined grain boundaries, highlighting strong metallurgical bonding essential for mechanical integrity and wear resistance. Figure 2(d) at 1000× shows regions where reinforcement particles appear segregated along grain boundaries, a result of solidification dynamics. Quantitative analysis indicates average interparticle spacing below 15 μm in most regions, with local increases to approximately 25–30 μm near grain boundaries, consistent with maintaining favorable tribological performance under dry sliding conditions.

## *Experimental design and test methods*

Selection of control parameters and their levels was based on a combination of literature survey, preliminary trials, and relevance to tribological behavior of AZ91-based hybrid composites. The four input variables considered, normal load, sliding speed, h-BN content, and sliding distance directly influence interfacial contact mechanics, heat generation, and lubrication phenomena. Load values from 10 N to 40 N and speeds from 1.0 to 2.5 m/s were chosen to span light to moderate tribological regimes. h-BN content varied from 0 to 1.5 wt.% to evaluate its influence as a solid lubricant in synergy with $TiB_2$. Sliding distance levels (1 and 2 km) captured both short and extended wear conditions. These factors and levels are listed in Table 2.

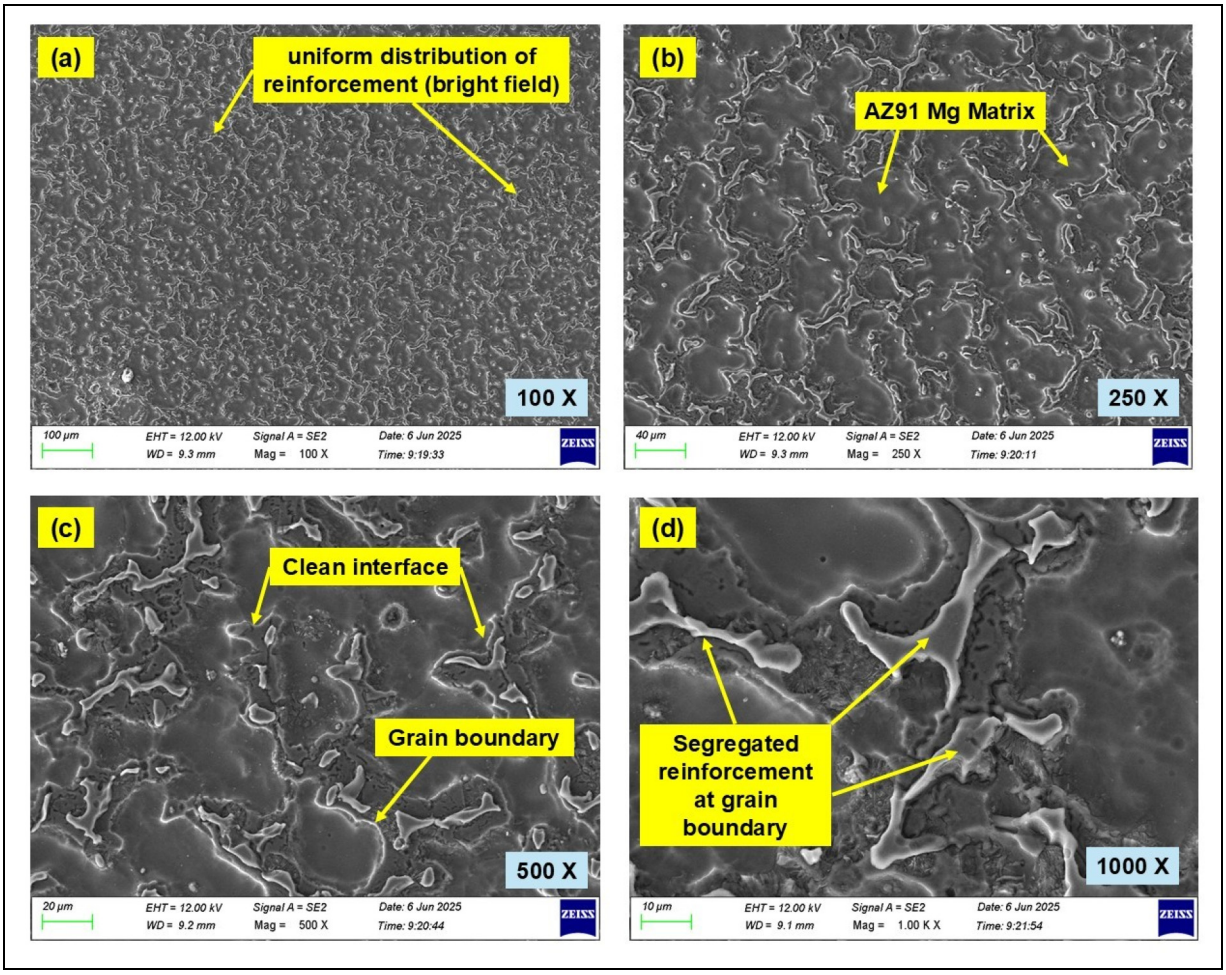


**Figure 2.** SEM images of AZ91/$TiB_2$–h-BN composites showing (a) uniform reinforcement distribution (100×), (b) continuous AZ91 Mg matrix (250×), (c) clean interfaces and grain boundaries (500×), and (d) segregated reinforcement along grain boundaries from solidification effects (1000×).

Experiments were designed using Taguchi's L16 orthogonal array showed in Table 3, which efficiently accommodates four factors with mixed levels while minimizing experimental effort. All tests were conducted under dry conditions at room temperature using a DUCOM pin-on-disc tribometer in accordance with ASTM G99 standards. Composite specimens were machined into cylindrical pins of 6 mm diameter and 40 mm length, with a hemispherical tip to ensure consistent point contact. The counter face was a stainless steel 316L disc, polished to a surface roughness below 5 µm to minimize variability due to surface topography. Frictional force was recorded continuously during each run, while mass loss was determined using a Shimadzu AUW-D dual-range semi-micro balance with 0.01 mg resolution to ensure high precision in wear rate calculation. Each experiment was repeated for consistency and data reliability.

**Table 2.** Factors and levels.

| Factors | Code | Levels |
|---|---|---|
| Normal load (N) | NL | 10, 20, 30 and 40 |
| Sliding speed (m/s) | SS | 1, 1.5, 2, and 2.5 |
| h-BN content (wt.%) | h-BN | 0, 0.5, 1 and 1.5 |
| Sliding distance (km) | SD | 1 and 2 |

The localized mechanical conditions imposed during the sliding wear tests were analyzed through Hertzian contact mechanics to determine the maximum contact stresses between the hemispherical AZ91/$TiB_2$–h-BN composite pin and the stainless steel 316L disc. For a sphere-on-flat configuration, the radius of the circular contact area 'a' is calculated using equation (1).

$$a = \left(\frac{3F_N R}{4E^*}\right)^{1/3} \tag{1}$$

where '$F_N$' is the applied normal load, '$R$' is the radius of the hemispherical pin, and '$E^*$' is the effective elastic modulus of the contacting pair. The maximum Hertzian contact pressure '$p_0$' at the center of the contact area is subsequently determined by equation (2).

$$p_0 = \frac{3F_N}{2\pi a^2} \tag{2}$$

The effective elastic modulus '$E^*$' accounts for the elastic properties of both the composite pin and the counterface and is expressed by equation (3).

$$\frac{1}{E^*} = \frac{1-\nu_1^2}{E_1} + \frac{1-\nu_2^2}{E_2} \tag{3}$$

where $E_1$ and $\nu_{1\ 1}$ are the Young's modulus and Poisson's ratio of the AZ91/$TiB_2$–h-BN composite, and $E_2$ and $\nu_2$

**Table 3.** Design of experiment L16 orthogonal array.

| Exp. run | Normal load (N) | Sliding speed (m/s) | h-BN (wt.%) | Sliding distance (km) |
|---|---|---|---|---|
| 1 | 10 | 1 | 0 | 1 |
| 2 | 10 | 1.5 | 0.5 | 1 |
| 3 | 10 | 2 | 1 | 2 |
| 4 | 10 | 2.5 | 1.5 | 2 |
| 5 | 20 | 1 | 0.5 | 2 |
| 6 | 20 | 1.5 | 0 | 2 |
| 7 | 20 | 2 | 1.5 | 1 |
| 8 | 20 | 2.5 | 1 | 1 |
| 9 | 30 | 1 | 1 | 1 |
| 10 | 30 | 1.5 | 1.5 | 1 |
| 11 | 30 | 2 | 0 | 2 |
| 12 | 30 | 2.5 | 0.5 | 2 |
| 13 | 40 | 1 | 1.5 | 2 |
| 14 | 40 | 1.5 | 1 | 2 |
| 15 | 40 | 2 | 0.5 | 1 |
| 16 | 40 | 2.5 | 0 | 1 |

**Table 4.** Hertzian contact stress values.

| Normal load (N) | Contact radius '$a$' (μm) | Maximum Hertzian contact stress ($p_0$) (MPa) |
|---|---|---|
| 10 | 78.9 | 765.46 |
| 20 | 99.5 | 964.42 |
| 30 | 113.9 | 1103.98 |
| 40 | 125.4 | 1215.09 |

correspond to the stainless steel 316L disc. Although the h-BN content in the present study was varied from 0 to 1.5 wt.% to investigate its influence on tribological performance, its relatively low volume fraction and moderate modulus result in minimal impact on the overall composite stiffness. Therefore, an average Young's modulus of 52 GPa and Poisson's ratio of 0.33 were adopted for the composite in the calculations, providing a practical and scientifically reasonable approximation across all formulations. For stainless steel 316L, a Young's modulus of 193 GPa and Poisson's ratio of 0.28 were employed. Substituting these values yields an effective elastic modulus of approximately 45.64 GPa. Considering the hemispherical pin geometry with a radius of 3 mm and varying applied loads, the computed contact radii and corresponding maximum Hertzian contact pressures are summarized in Table 4. These calculated stresses, ranging from approximately 765 MPa to 1215 MPa, indicate that the sliding tests were conducted under conditions capable of generating significant local plastic deformation and tribo-mechanical interactions.

## Results and discussion

### Taguchi analysis

Taguchi's S/N ratio framework was employed to quantify the influence of control parameters on the wear performance of AZ91/$TiB_2$-hBN composites, adopting the "smaller-is-better" criterion. The main effect plot in Figure 3 illustrates the variation in mean S/N ratios for wear rate with respect to each factor. Normal load had the most significant influence, evidenced by a steep negative slope. As the load increased from 10 N to 40 N, wear performance deteriorated due to intensified contact stress, which led to plastic deformation of the AZ91 matrix, microfracture at the reinforcement–matrix interface, and potential delamination of the embedded ceramic particles. These effects were further aggravated by localized thermal softening and increased oxidative wear at the higher loads.

Sliding speed had a relatively minor influence within the studied range. However, a slight improvement in wear resistance around 2 m/s can be attributed to optimal dynamic conditions that may reduce debris entrapment and enhance the stability of any tribo-chemical film formed. In contrast, excessive speeds beyond this threshold did not provide further gains, likely due to increased thermal accumulation and matrix softening.

The h-BN content strongly affected the wear behavior. The progressive increase in S/N ratio from 0 to 1.5 wt.% h-BN confirmed its effectiveness in enhancing wear resistance. As a lamellar solid lubricant, h-BN acts as a barrier against direct metal-to-metal contact, facilitating easy interfacial shearing and reducing abrasive plowing. Its dispersion alongside $TiB_2$ also promotes a dual-mechanism of load bearing (via $TiB_2$) and lubricating (via h-BN) functions. Sliding distance exhibited a marginal impact; however, shorter distances (1 km) consistently showed slightly higher S/N ratios. This trend may be due to limited thermal accumulation and reduced surface fatigue, which preserved the integrity of the protective tribo-film during shorter test durations.

The interaction plots illustrated in Figure 4 for wear rate reveal pronounced non-linear interdependencies among the process variables, highlighting the complex nature of tribological performance in AZ91/$TiB_2$-hBN composites. A particularly notable trend is the combination of low normal loads (10–20 N) with high h-BN contents (1.0–1.5 wt.%), which consistently yields the lowest wear rates. This behavior reflects an optimized synergy between the load-bearing capacity of $TiB_2$ and the interfacial lubricity imparted by h-BN. Under moderate mechanical stress, the AZ91 matrix retains its structural stability, allowing the $TiB_2$ particles to remain well-anchored and effective in minimizing direct metal contact, while the lamellar h-BN layers shear easily at the interface, reducing friction-induced abrasion and limiting matrix degradation.

However, as the normal load increases beyond 30 N, the effectiveness of h-BN begins to diminish despite its solid lubricating nature. This deterioration in wear resistance under higher loads may be attributed to several factors: (i) mechanical disintegration or exfoliation of the h-BN tribo-film due to intensified shear forces, (ii) partial particle debonding or pull-out, especially in regions with poor interfacial wettability, and (iii) the onset of microstructural damage in the matrix–reinforcement interface, which disrupts the stability of the protective tribo-layer. These effects collectively promote three-body abrasion and oxidative wear, overshadowing the intended tribological benefits of h-BN at elevated stress conditions.

The coefficient of friction behavior, depicted in Figure 5, corroborates these findings. The presence of h-BN significantly lowers COF across all tested speeds and loads, a result of its graphitic-like structure that provides a low-resistance shear plane between the sliding surfaces. The layered hexagonal lattice of h-BN, analogous to $MoS_2$ or graphite,

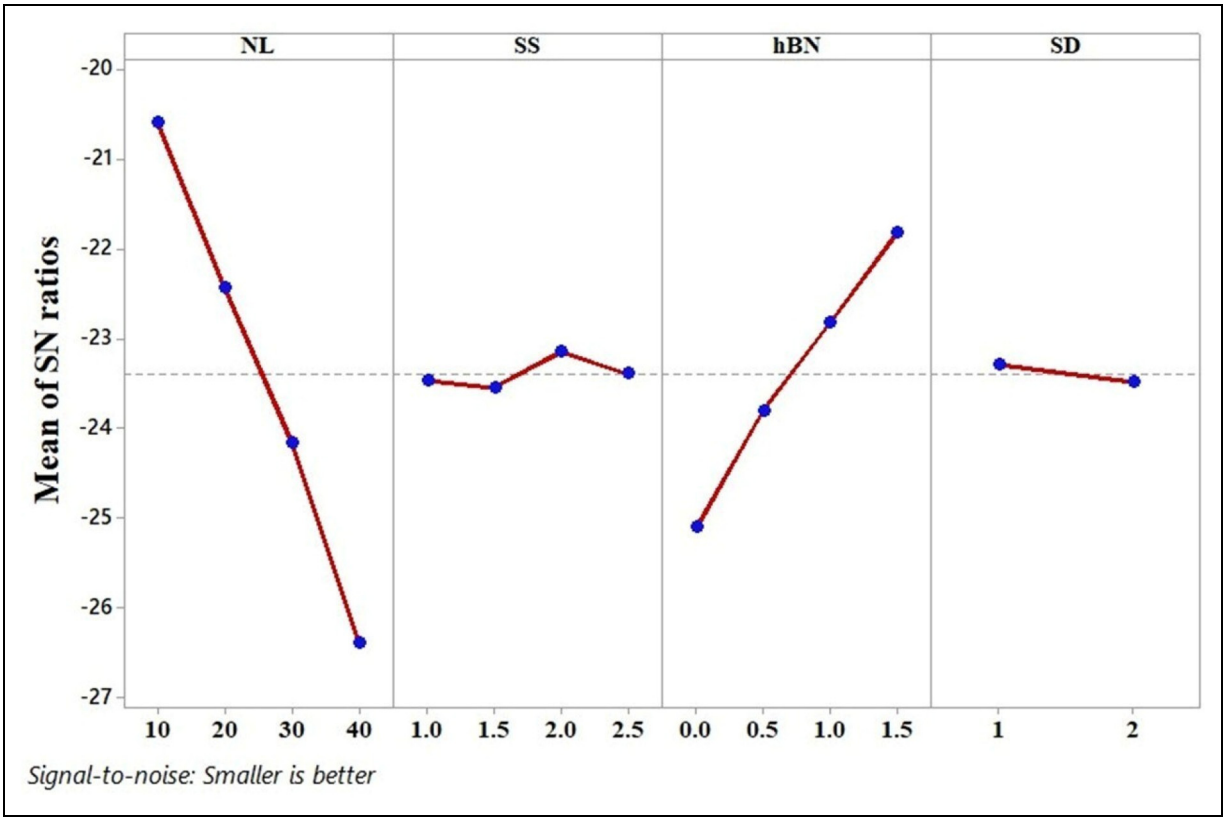


**Figure 3.** Main effect plots for mean S/N ratios showing the influence of normal load, sliding speed, h-BN content, and sliding distance on wear rate in AZ91/$TiB_2$–h-BN composites.

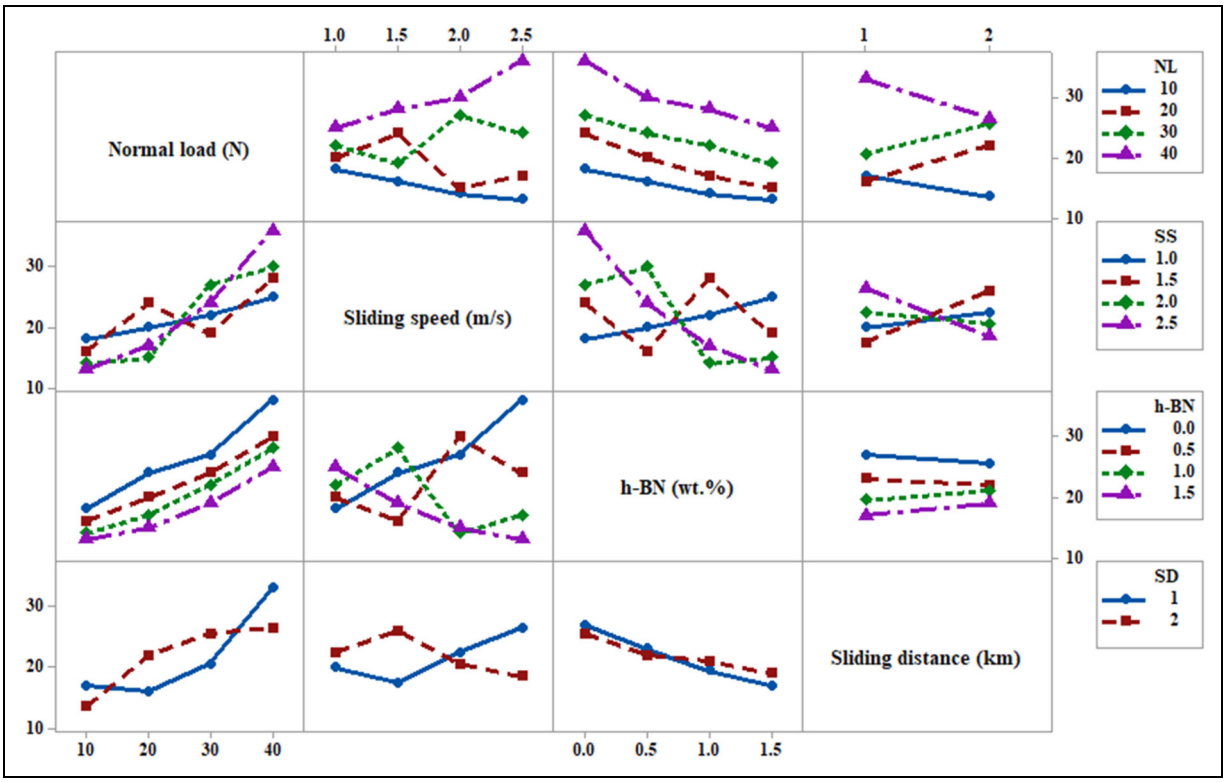


**Figure 4.** Interaction plots illustrating combined effects of normal load, sliding speed, h-BN content, and sliding distance on wear rate in AZ91/$TiB_2$–h-BN composites.

facilitates easy interfacial displacement, effectively reducing the adhesive component of friction and supporting smoother sliding. However, this benefit is not indefinite. At higher sliding speeds (≥2 m/s) or extended sliding distances, there is a subtle increase in COF, suggesting a compromise in film integrity. Thermal softening of the matrix, oxidative

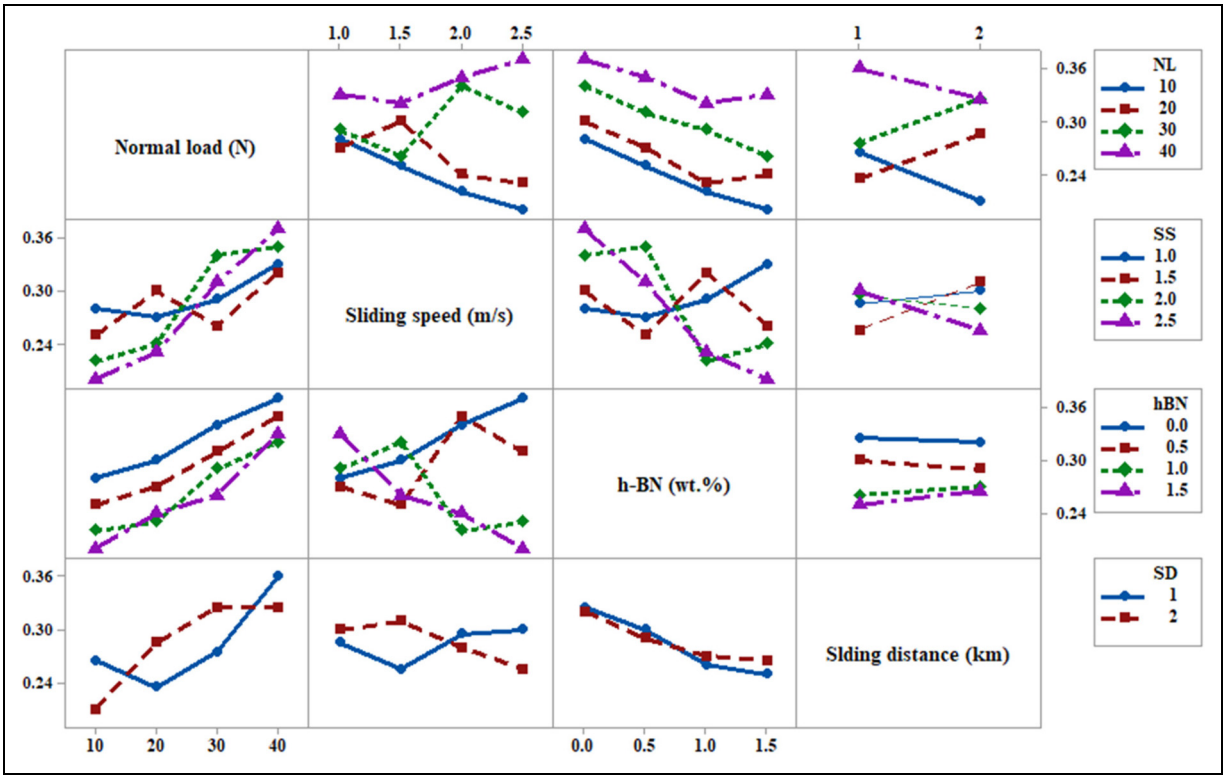


**Figure 5.** Interaction plots illustrating combined effects of normal load, sliding speed, h-BN content, and sliding distance on coefficient of friction in AZ91/$TiB_2$–h-BN composites.

degradation, and tribo-chemical transformation of h-BN layers could contribute to this reversal, resulting in intermittent breakdown of the lubricating film and a transition to mixed or boundary lubrication regimes.

## *Gradient boosting regression (GBR) modeling*

Modeling the wear rate and coefficient of friction (COF) responses of AZ91/$TiB_2$-hBN composites requires capturing the inherent non-linear dependencies among multiple process variables. Traditional regression techniques often fall short in representing such complexities. In the present study, Gradient Boosting Regression (GBR) was implemented, owing to its sequential learning capability and robustness against overfitting. The conceptual framework of the GBR model, as shown in Figure 6, illustrates the iterative training mechanism where successive decision trees are built to correct the residuals of preceding trees, optimizing prediction accuracy at each stage. The GBR models were developed with hyperparameters optimized through grid search. For wear rate prediction, the learning rate was set at 0.1, maximum depth at 1, and 100 estimators were used. For COF, 150 estimators were employed while maintaining the same learning rate and depth. The training dataset comprised normal load, sliding speed, h-BN content, and sliding distance as inputs, and wear rate (mg/km) and COF as outputs.

Validation of the developed models was performed through actual versus predicted plots shown in Figure 6. The model achieved an $R^2$ value of 0.816 for wear rate prediction (Figure 7(a)) and 0.825 for COF prediction (Figure 7(b)), confirming excellent agreement with experimental data. The clustering of data points along the 45° reference line demonstrates that the model captures the underlying trends with high fidelity, ensuring its applicability for predictive analysis and optimization.

The feature importance plot presented in Figure 8 highlights the contribution of each input parameter toward the model predictions. For wear rate, normal load was identified as the most influential factor, followed by h-BN content, sliding speed, and sliding distance. This ranking is physically intuitive, as higher normal loads intensify the mechanical interaction at the contact interface, directly influencing material removal. In the case of COF prediction, h-BN content emerged as the most dominant factor, reflecting the pivotal role of solid lubrication in reducing interfacial shear stress.

Training and validation loss curves shown in Figure 9(a) (wear rate) and Figure 9(b) (COF) illustrate the learning behavior of the GBR models. The monotonic decrease in both training and validation losses without significant divergence confirms the absence of overfitting. For wear rate prediction, the loss stabilized after approximately 80 estimators, while for COF, convergence was achieved around 120–130 estimators, reflecting the slightly more complex relationship governing frictional behavior.

The error histograms depicted in Figure 9(c) and 9(d) further validate the predictive capability of the models. For wear rate (Figure 9(c)), the residuals were symmetrically distributed about zero with minimal dispersion, indicating low bias and reliable predictions. Similarly, for COF (Figure 9(d)), the narrow spread of residuals affirms the model's precision in friction estimation. These results demonstrate that the GBR model effectively captures the stochastic variations in experimental tribological data without systematic errors.

The quantitative performance metrics, summarized in Table 5, reinforce the robustness of the developed models. For

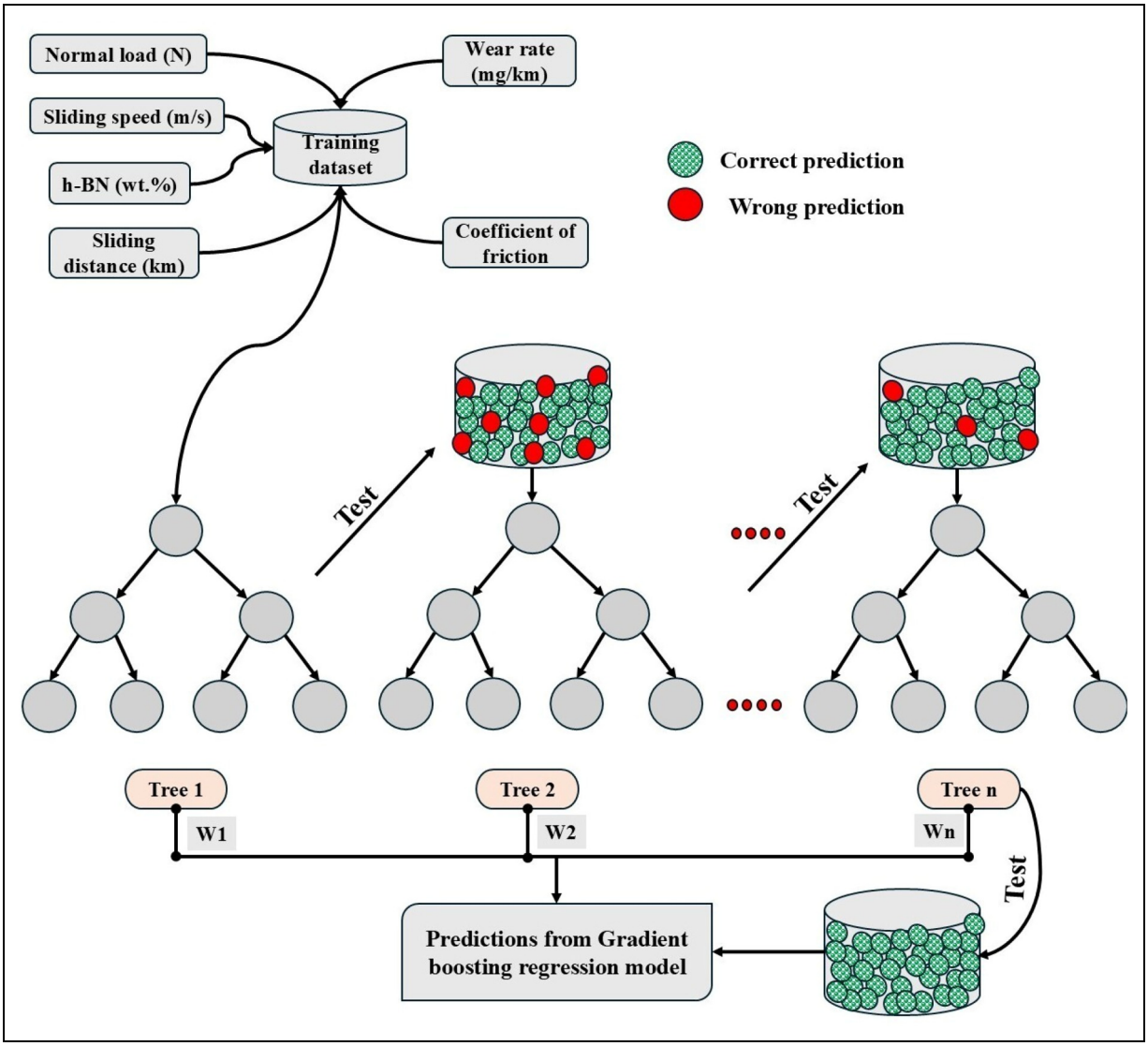


**Figure 6.** Conceptual architecture of the gradient boosting regression model used to predict wear rate and coefficient of friction in AZ91/$TiB_2$–h-BN composites.

wear rate, the model achieved a cross-validation $R^2$ of 0.8697, a test-set $R^2$ of 0.8160, and an MSE of 5.5185 mg²/km². For COF, the cross-validation $R^2$ was 0.5633 with a higher test-set $R^2$ of 0.8246 and an MSE of 0.000232.

Although COF prediction exhibited slightly lower cross-validation performance, the final testing accuracy remained high, reflecting the model's generalization capability despite complex tribo-chemical and thermal interactions. The GBR models developed in this study offer a powerful predictive tool for simultaneously modeling wear and frictional responses in AZ91/$TiB_2$-hBN composites. Their integration with optimization frameworks further enables intelligent exploration of process parameter space for enhanced tribological performance under dry sliding conditions.

## *Optimization using multi-objective particle swarm optimization (MOPSO)*

Efficient optimization of tribological performance parameters in hybrid AZ91/$TiB_2$-hBN composites demands a multi-objective approach that can simultaneously minimize wear rate and coefficient of friction (COF). Given the non-linear relationships between input parameters and output responses modelled through Gradient Boosting Regression (GBR), Multi-Objective Particle Swarm Optimization (MOPSO) was employed. MOPSO offers an inherent capability to maintain solution diversity along the Pareto front while converging towards optimal regions, making it ideal for handling the conflicting objectives of reducing both wear and friction.

The workflow of the developed MOPSO framework is illustrated in Figure 10. Experimental data was first used to fit surrogate GBR models for wear rate and COF. Key MOPSO parameters included a swarm size of 30 particles, 50 iterations, inertia weight (w) of 0.7, cognitive coefficient (C1) of 1.5, and social coefficient (C2) of 1.5. The decision variables normal load (N), sliding speed (m/s), $TiB_2$ content (wt.%), and sliding distance (km) were bounded according to the experimental domain to ensure practical feasibility.

The parameters selected for the Multi-Objective Particle Swarm Optimization (MOPSO) algorithm, specifically a swarm size of 30 particles, 50 iterations, inertia weight of 0.7, and cognitive and social coefficients both set at 1.5, were chosen to balance computational efficiency with

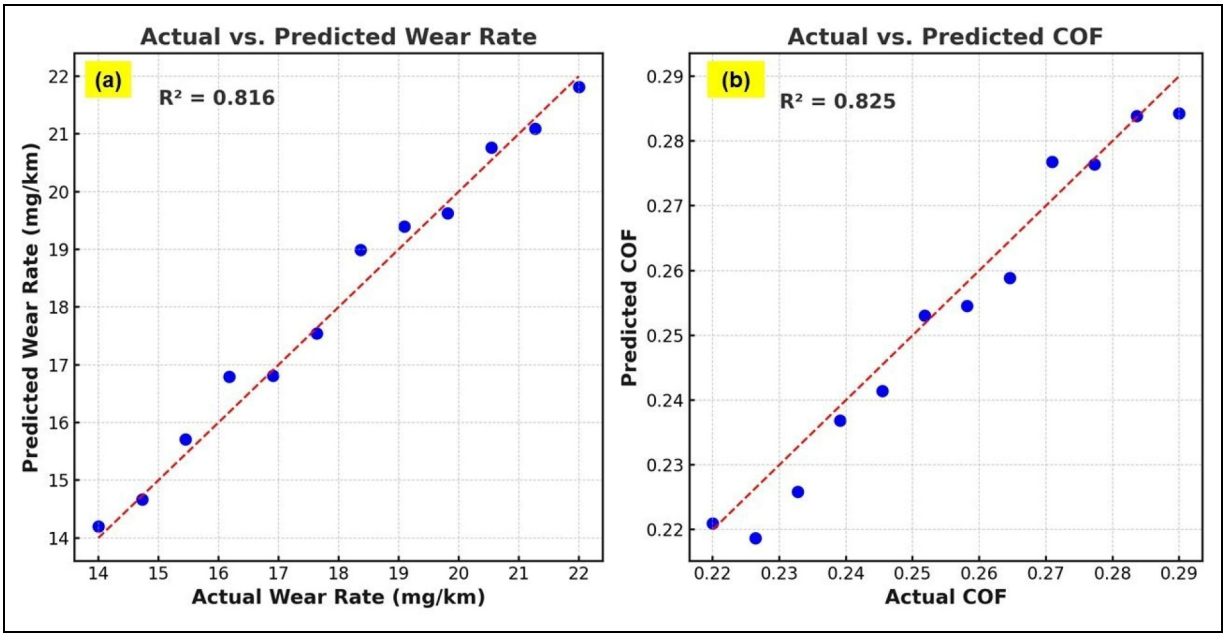


**Figure 7.** Actual versus predicted plots showing model accuracy for (a) wear rate and (b) coefficient of friction predictions in AZ91/$TiB_2$–h-BN composites using gradient boosting regression.

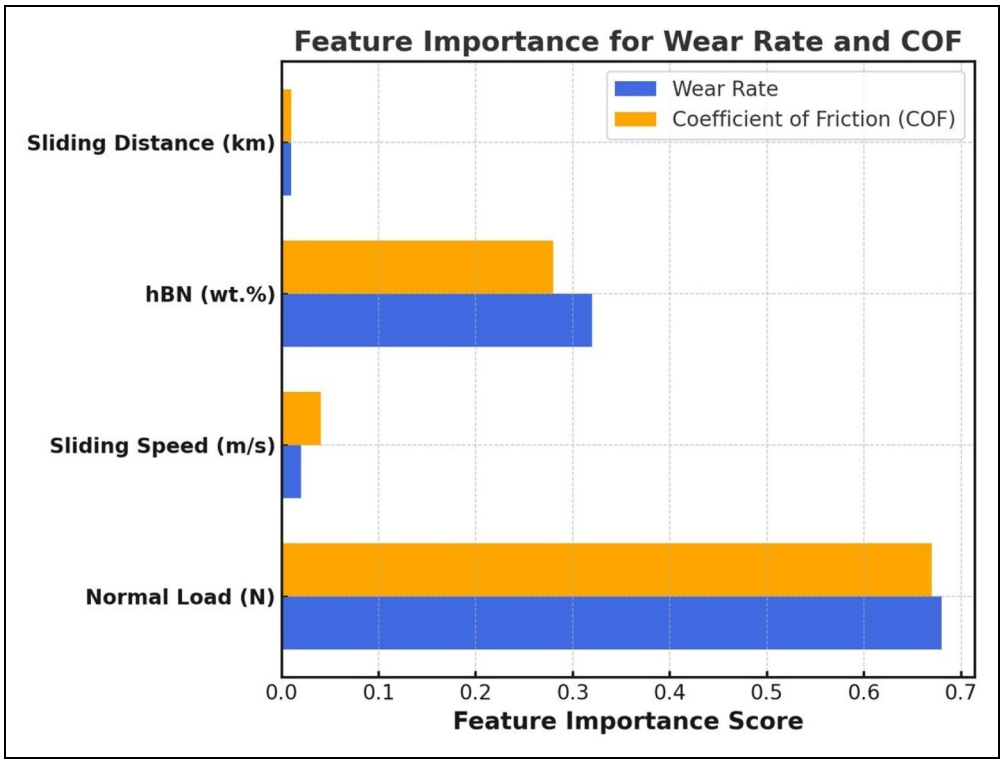


**Figure 8.** Feature importance plots for (a) wear rate and coefficient of friction predictions in AZ91/$TiB_2$–h-BN composites, indicating the relative influence of input parameters in the gradient boosting regression model.

sufficient exploration of the high-dimensional design space defined by the four decision variables in this study. A swarm size of 30 provides adequate diversity to capture multiple Pareto-optimal solutions without imposing excessive computational load, which is critical when surrogate models such as Gradient Boosting Regression (GBR) are evaluated iteratively during optimization.

The iteration counts of 50 was determined based on preliminary convergence analyses, where no significant improvement in the Pareto front was observed beyond this point. The inertia weight of 0.7 was selected to balance exploration and exploitation, ensuring particles do not converge prematurely while still allowing the swarm to refine local optima. Cognitive (C1) and social (C2) coefficients were both fixed at 1.5 to maintain an equilibrium between personal experience (local search) and collective swarm knowledge (global search), a configuration demonstrated to be effective in many multi-objective optimization contexts.

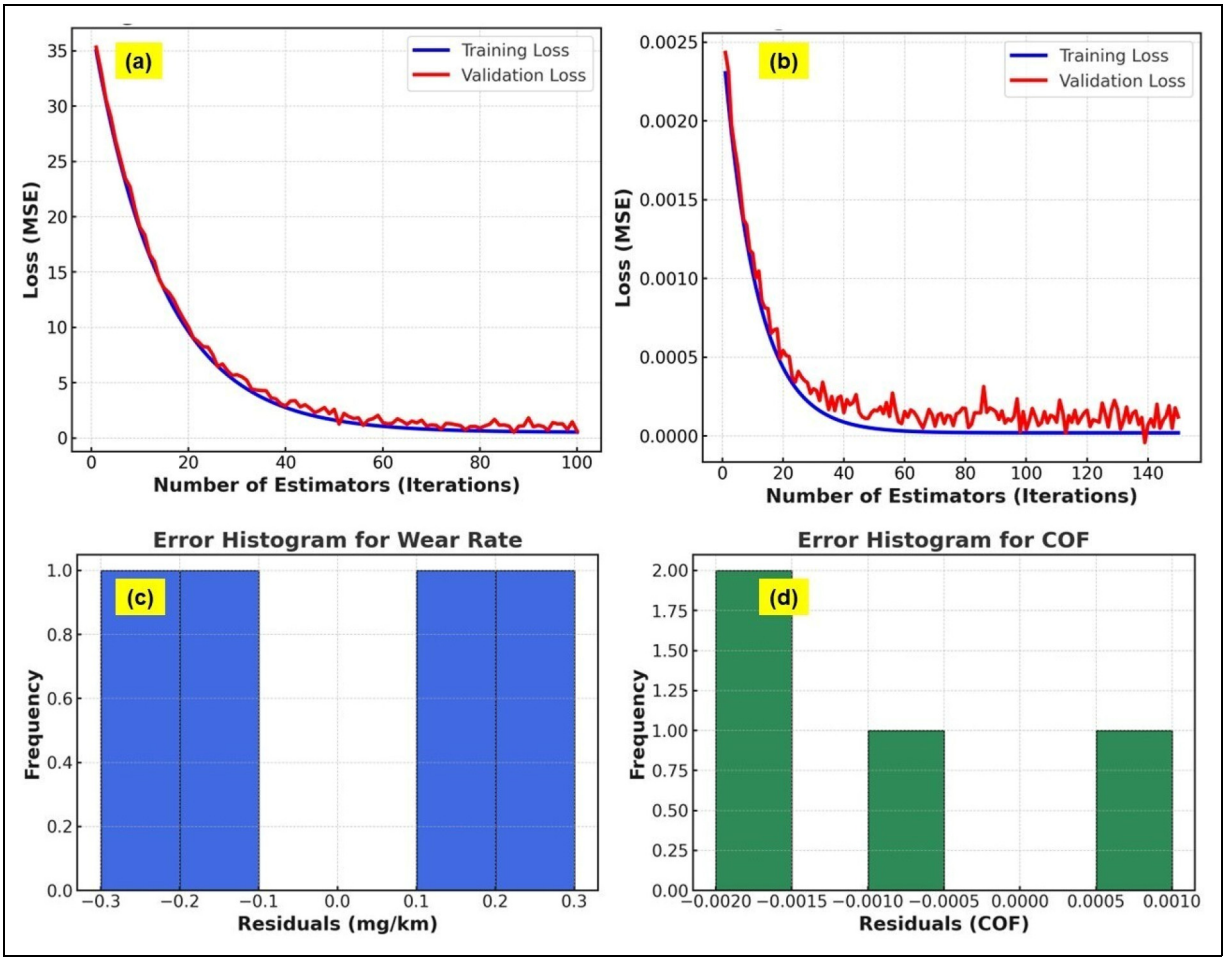


**Figure 9.** (a) & (b) Training and validation loss plots for wear rate and coefficient of friction, and (c) & (d) error histograms illustrating residual distributions for wear rate and coefficient of friction predictions in AZ91/$TiB_2$–h-BN composites using gradient boosting regression.

These parameter choices ensured stable convergence behavior and robust identification of Pareto-optimal solutions for wear rate and coefficient of friction, while maintaining computational tractability.

The velocity and position of particles were updated using the classical PSO equations (1) and (2) as represented below.

$$v_i^{k+1} = wv_i^k + c_1 r_1(pbest_i - x_i^k) + c_2 r_2(gbest - x_i^k) \quad (1)$$

$$x_i^{k+1} = x_i^k + v_i^{k+1} \quad (2)$$

where $v_i$ and $x_i$ denote the velocity and position of particle '$i$', respectively, $pbest_i$ is the personal best position, and $gbest$ is the global best leader selected from an external non-dominated archive.

Predicted values of wear rate and COF were computed for each particle using the GBR surrogate models. Non-dominated solutions were stored and updated iteratively. The optimization algorithm terminated upon reaching the maximum number of iterations or achieving stagnation in Pareto front improvement. Validation of the surrogate-assisted MOPSO optimization was confirmed through the previously developed GBR models, with $R^2$ values of 0.816 for wear rate and 0.825 for COF, as discussed in Section 3.2. The convergence behavior was smooth, indicating efficient exploration and exploitation of the design space. The optimized process parameters corresponding to varying weightage between wear rate and COF minimization objectives are summarized in Table 6.

The optimized solutions reveal that lower sliding speeds (~1.0–1.0076 m/s), higher h-BN content (~1.17 wt.%), and minimum sliding distance (1 km) consistently emerged as favorable conditions. Normal load remained high (40 N) across all optimal settings, implying that once sufficient h-BN is incorporated to establish an effective solid lubricant layer, higher loads become manageable without severe wear escalation. The slight increase in predicted wear rate when shifting weightage towards COF minimization is an expected trade-off, highlighting the Pareto nature of the solution set. The optimized results underscore the critical role of solid lubrication (h-BN) combined with controlled mechanical loading to achieve simultaneous minimization of wear and friction in AZ91/$TiB_2$-hBN composites. This strategic process parameter tuning, supported by GBR and MOPSO frameworks, offers a pathway toward developing high-performance lightweight materials for dry sliding applications.

## *Confirmation test and characterization*

A confirmation test was conducted using the optimized process parameters obtained from the surrogate-assisted MOPSO optimization. The identified optimal settings were normal load = 40 N, sliding speed = 1.00 m/s, h-BN

**Table 5.** Performance metrics of the gradient boosting regression (GBR) models.

| Response | Cross-validation $R^2$ | Test-set $R^2$ | Mean squared error (MSE) | Root mean squared error (RMSE) | Mean absolute error (MAE) |
|---|---|---|---|---|---|
| Wear Rate (mg/km) | 0.8697 | 0.816 | 5.5185 | 2.348 | 1.9215 |
| Coefficient of Friction (COF) | 0.5633 | 0.8246 | 0.000232 | 0.0152 | 0.0127 |

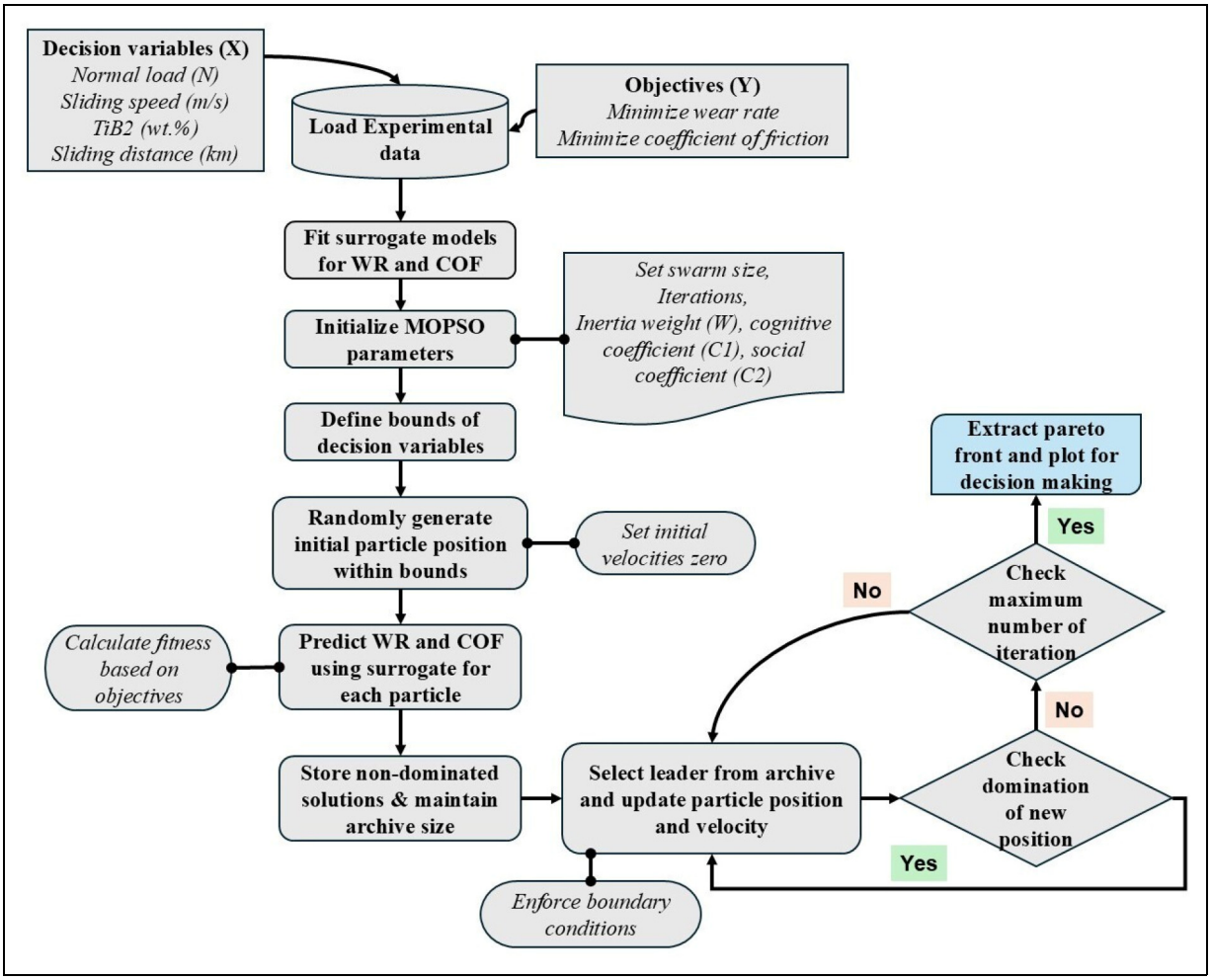


**Figure 10.** Methodology flowchart of the multi-objective particle swarm optimization (MOPSO) process used to optimize wear rate and coefficient of friction in AZ91/$TiB_2$–h-BN composites.

content = 1.1731 wt.%, and Sliding distance = 1 km. The objective was to validate the predictive capability of the MOPSO-GBR framework by comparing the experimental responses with the predicted outputs for wear rate and coefficient of friction (COF). The comparison of experimental and predicted results, along with the percentage deviation, is summarized in Table 7. The deviations observed were within ±5%, indicating excellent predictive reliability and confirming the robustness of the developed surrogate models and optimization methodology.

The slight positive deviation in wear rate and COF can be attributed to inherent experimental variability such as minor inconsistencies in surface finishing, environmental fluctuations, and third-body effects during sliding. Post-testing, the worn surface of the specimen fabricated under optimized conditions was examined using scanning electron microscopy (SEM), as shown in Figure 11. The SEM analysis provided critical insights into the prevailing wear mechanisms and the efficacy of the hybrid reinforcement system.

Figure 11(a) illustrates the presence of abrasive grooves along with dispersed adhered debris particles. The grooves indicate a micro-cutting mechanism predominantly governed by the hard $TiB_2$ particles acting against the counterface, while adhered debris signifies localized adhesive interactions during sliding. In Figure 11(b), a distinct tribolayer is visible along with delaminated oxide fragments. Formation of a tribolayer suggests beneficial third-body protection, where oxidized layers reduce direct metal-to-metal contact and stabilize friction, enhancing wear resistance.

Figure 11(c) reveals microgrooves and surface cracks, implying a combination of micro-abrasive and fatigue-induced wear. Crack propagation along the sliding direction could be a consequence of repetitive stress cycles and strain localization in the soft AZ91 matrix beneath the

**Table 6.** Optimum process parameters and responses from MOPSO.

| Weights (wear rate: COF) | Normal load (N) | Sliding speed (m/s) | h-BN content (wt.%) | Sliding distance (km) | Predicted wear rate (mg/km) | Predicted COF |
|---|---|---|---|---|---|---|
| (1.0, 0.0) | 40 | 1 | 1.1731 | 1 | 14.129 | 0.2632 |
| (0.75, 0.25) | 40 | 1.0076 | 1.1731 | 1 | 14.298 | 0.2567 |
| (0.50, 0.50) | 40 | 1.0076 | 1.1731 | 1 | 14.423 | 0.2493 |
| (0.25, 0.75) | 40 | 1.0076 | 1.1731 | 1 | 14.565 | 0.2421 |
| (0.0, 1.0) | 40 | 1.0076 | 1.1731 | 1 | 14.703 | 0.2352 |

reinforced layer. Figure 11(d) highlights the accumulation of debris clusters and significant adhered debris, indicative of limited debris ejection capability at optimized conditions. Such clustered debris might act intermittently as an abrasive third body, slightly contributing to the overall wear rate without destabilizing the tribolayer.

A well-developed smooth track is observed in Figure 11(e), accompanied by signs of surface flow. This morphology suggests that under optimized parameters, the synergistic effect of $TiB_2$ load support and h-BN lubrication facilitated a ductile flow of the AZ91 matrix, minimizing abrasive wear and promoting smoother sliding. Finally, Figure 11(f) depicts localized debris accumulation near the grooves, possibly trapped within micro-asperities. While debris accumulation typically promotes plowing-type wear, the limited accumulation seen here corroborates the relatively low wear rates measured experimentally.

The worn surface morphology confirms that the hybrid reinforcement strategy combining hard $TiB_2$ particles and lubricating h-BN flakes effectively mitigates severe adhesive and abrasive damage mechanisms. The optimized parameters ensured stable tribolayer formation, effective debris management, and minimal crack propagation, aligning well with the objectives of reducing both wear rate and coefficient of friction. Thus, the confirmation test validates that the integration of GBR modeling and MOPSO optimization provides a robust framework for predicting and improving the dry sliding tribological performance of AZ91/$TiB_2$-hBN hybrid composites.

The solid lubrication behavior of h-BN observed in the present AZ91/$TiB_2$–h-BN composites align with broader findings in the literature where various solid lubricants have been integrated into magnesium-based systems to mitigate wear and reduce friction through tribolayer formation and interfacial shear reduction. For instance, Ayyanar S et al. reported that incorporating up to 7.5 wt.% $WS_2$ into AZ91D magnesium alloys significantly improved wear resistance by developing a self-lubricating tribolayer that curtailed oxidation and adhesive wear under dry sliding conditions.[32] Similarly, Narayanasamy P et al. demonstrated that $MoS_2$ outperformed graphite as a solid lubricant in magnesium composites, where Mg–10$MoS_2$ exhibited superior mechanical strength and lower wear loss due to uniform dispersion and effective interfacial lubrication.[33] K.T. Aliasker et al. further substantiated the beneficial role of $MoS_2$, showing that up to 6 vol.% introduced via friction stir processing enhanced both hardness and wear resistance, though higher contents slightly compromised corrosion resistance and ductility.[34] Y.L. Yin et al. found that serpentine-structured MSH nanotubes used as oil additives achieved friction reductions between 18.7–68.5% and wear reductions of 19.4–54.3% in AZ91D, attributing the improvements to the formation of a hard, lubricious tribolayer that acted as a barrier against severe surface damage.[35] Ridvan Kucukosman et al. observed that graphene oxide incorporated into PEO coatings on AZ91 magnesium alloys formed a thin, adherent film that significantly enhanced hardness and wear resistance, particularly after hydrothermal treatment, suggesting a dual mechanism of mechanical reinforcement and interfacial lubrication.[36] Likewise, Yashar Behnamian showed that incorporating 0.5 wt.% multi-walled carbon nanotubes (MWCNTs) into ZK60 magnesium composites reduced friction and wear rates, with optimal performance achieved in hybrids containing both $B_4C$ and MWCNTs, highlighting the synergy between hard reinforcements and lubricating phases.[37] Sandeep Kumar Khatkar et al. reported that graphite additions to AZ91D–SiC composites improved wear resistance through the development of a lubricating layer, though the applied load remained a dominant factor in determining wear performance.[38]

Compared to these studies, the present work uniquely leverages h-BN's lamellar crystal structure, which provides an inherently low interlayer shear strength, to reduce friction coefficients while simultaneously preserving mechanical integrity when combined with $TiB_2$ as a hard load-bearing phase. The observed wear mechanisms, including micro-grooving, tribolayer formation, and debris-controlled wear, confirm that h-BN operates analogously to other solid lubricants by facilitating interfacial sliding and mitigating direct metal-to-metal contact under dry sliding. However, unlike certain lubricants such as $WS_2$ and $MoS_2$ that can undergo chemical transformations at elevated temperatures, h-BN exhibits excellent thermal stability, making it particularly advantageous for high-temperature tribological applications. Thus, the present findings not only substantiate the solid lubrication role of h-BN but also position it as a competitive alternative to traditional solid lubricants, combining low friction performance with thermal resilience and minimal impact on corrosion resistance in magnesium-based hybrid composites.

**Table 7.** Results of confirmation test and deviation with experimental results.

| Parameter | Predicted value | Experimental value | Deviation (%) |
|---|---|---|---|
| Wear Rate (mg/km) | 14.565 | 14.98 | 2.77 |
| Coefficient of Friction (COF) | 0.2421 | 0.2517 | 3.81 |

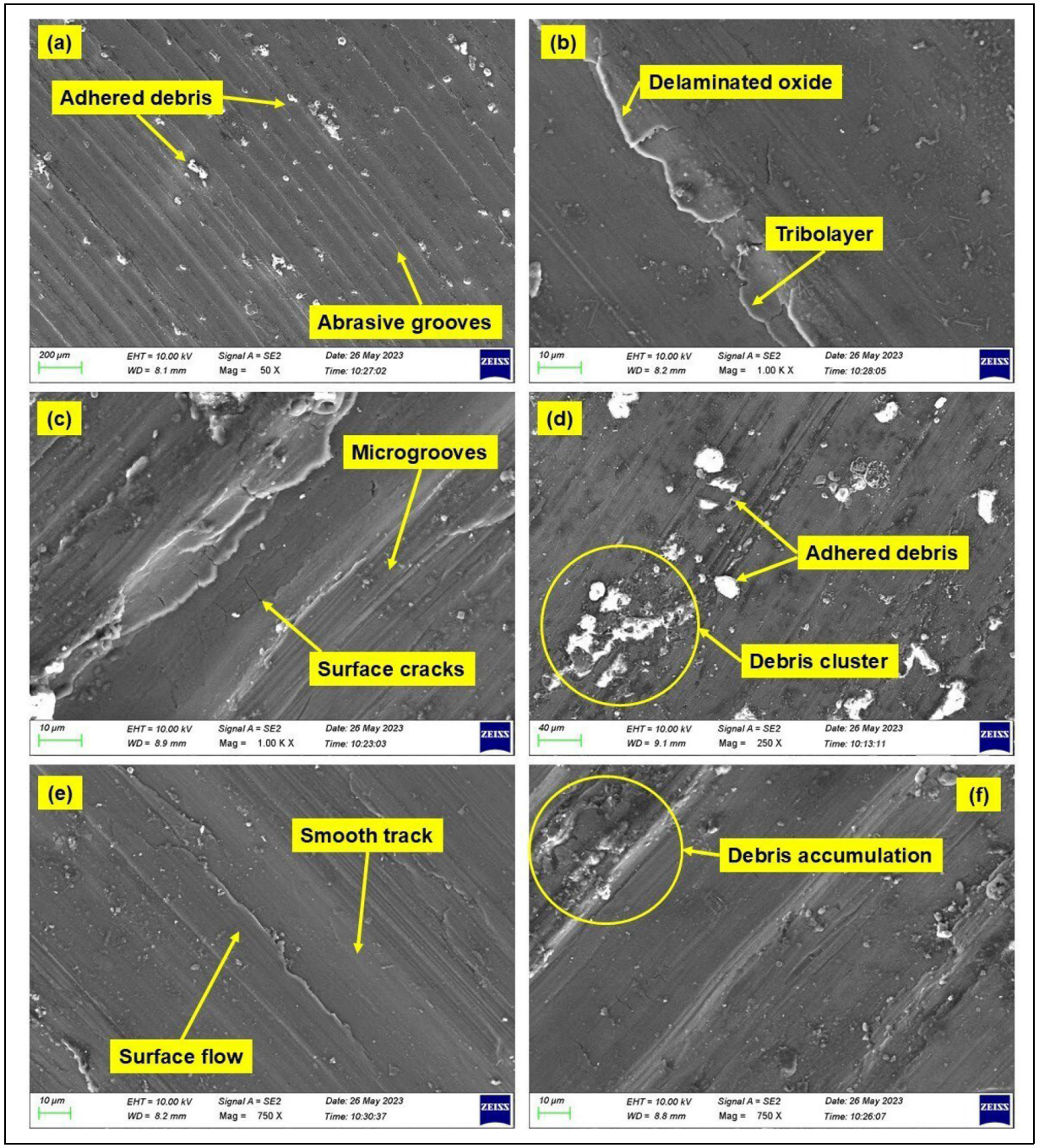


**Figure 11.** SEM images of worn surfaces from AZ91/$TiB_2$–h-BN composites: (a) abrasive grooves and adhered debris from micro-cutting, (b) tribolayer and delaminated oxide indicating protective film, (c) microgrooves and surface cracks, (d) adhered debris clusters, (e) smooth track with surface flow, and (f) localized debris accumulation.

Beyond traditional casting methods, recent advances in solid-state processing techniques such as friction stir processing (FSP) have further highlighted the benefits of hybrid reinforcement and solid lubricants in light-metal composites. Min Ling et al. demonstrated that AZ61 magnesium surface composites fabricated with $CeO_2$ and $ZrO_2$ via FSP under water-cooled conditions exhibited finer grain structures, increased hardness, and reduced wear rates compared to air-processed counterparts, emphasizing the role of thermal management in microstructural control.[39] Yang Zhang et al. showed that a protruding cylindrical tool in FSP significantly improved the dispersion of h-BN and $ZrO_2$ in AA5754 aluminum, achieving enhanced surface integrity, refined grains, and improved shear strength and wear resistance, illustrating how tool geometry influences reinforcement distribution and tribological performance.[40] Furthermore, Zhaoyang Zuo et al. incorporated h-BN as a solid lubricant in AZ31 magnesium composites through vibrational-assistance FSP, achieving a 40% reduction in wear rate alongside improved grain refinement, hardness, and shear strength relative to conventional processing.[41] Although the present study utilizes stir casting rather than FSP, these works collectively underscore the broader significance of combining ceramic reinforcements and solid lubricants such as h-BN to tailor microstructure and enhance the tribological performance of magnesium-based composites.

## Conclusion

This study comprehensively investigated the dry sliding tribological behavior of AZ91 magnesium alloy reinforced with $TiB_2$ and h-BN ceramic particles, focusing on optimizing wear rate and coefficient of friction (COF) through a novel hybrid modeling–optimization approach integrating Gradient Boosting Regression (GBR) and Multi-Objective Particle Swarm Optimization (MOPSO). Unlike prior studies that typically addressed either experimental wear behavior or modeling in isolation, this work uniquely combines experimental validation, advanced machine learning, and multi-objective optimization within a single framework, delivering a more holistic understanding and predictive capability for tribological performance. The following conclusions were drawn:

- Hybrid AZ91/$TiB_2$–hBN composites were successfully fabricated via two-stage stir casting, integrating mechanical and ultrasonic stirring to ensure uniform dispersion of reinforcements, a process seldom coupled with machine learning optimization in earlier works.
- Taguchi analysis identified normal load and h-BN content as the most influential parameters controlling wear rate and COF, respectively, under dry sliding conditions, confirming and extending trends reported in earlier magnesium composite studies.
- The GBR model demonstrated high predictive accuracy with $R^2$ values of 0.816 for wear rate and 0.825 for COF, outperforming simpler regression methods used in previous research and capturing the complex non-linear interactions among process parameters.
- The MOPSO technique efficiently identified Pareto-optimal process parameters, leading to a minimum experimental wear rate of 14.98 mg/km and COF of 0.2517, with deviations less than 4% from predicted values, demonstrating the practical applicability of combining machine learning models with advanced multi-objective optimization—a strategy not commonly reported for AZ91-based systems.
- SEM analysis provided detailed insights into dominant wear mechanisms, revealing abrasive micro-grooving, tribolayer formation, and debris-controlled wear, thereby validating the hybrid reinforcement's synergistic role in enhancing both load-bearing capacity and solid lubrication.
- The study established that higher h-BN content (~1.17 wt.%) and lower sliding speed (~1.0 m/s) are crucial for achieving optimal tribological performance, a finding that refines the understanding of solid lubricant behavior in hybrid magnesium composites compared to prior works.
- The developed GBR–MOPSO hybrid framework represents a significant advancement, offering a robust predictive–optimization strategy that enables precise tailoring of tribological properties in lightweight metal matrix composites, distinguishing this work as a comprehensive contribution beyond conventional experimental optimization approaches.

Future research can extend these findings by investigating the high-temperature and wet-environment tribological behavior of AZ91/$TiB_2$–hBN composites, evaluating long-term durability under cyclic loading, and integrating real-time monitoring techniques such as acoustic emission analysis during sliding. Additionally, exploring deep learning architectures could further enhance predictive accuracy for broader tribological applications.

### ORCID iDs

Hariharasakthisudhan Ponnarengan https://orcid.org/0000-0002-9420-3196

Sathickbasha Katharbasha https://orcid.org/0000-0001-8974-154X

### Author contributions

- Sathish K: Investigation, Methodology, Data Curation, Formal Analysis, Writing – Original Draft Preparation.
- Baskar S (Secondary Corresponding Author): Conceptualization, Supervision, Project Administration, Validation, Writing – Review & Editing.
- Hariharasakthisudhan P (Primary Corresponding and Submitting Author): Conceptualization, Formal Analysis, Methodology, Writing – Review & Editing, Visualization.
- Logesh K: Software, Modeling, Data Validation, Resources, Writing – Review & Editing.
- Sathickbasha K: Experimental Setup, Data Curation, Investigation, Writing – Review & Editing.

### Funding

The authors received no financial support for the research, authorship, and/or publication of this article.

### Declaration of conflicting interests

The authors declared no potential conflicts of interest with respect to the research, authorship, and/or publication of this article.

### Data availability statement

The data supporting the findings of this study are available from the corresponding author upon reasonable request.

### References

1. Khatkar SK. Hybrid magnesium matrix composites: a review of reinforcement philosophies, mechanical and tribological characteristics. *Rev Adv Mater Sci* 2023; 62: 20220294.
2. Aydin F. Tribological aspects of magnesium matrix composites: a review of recent experimental studies. *Tribology-Materi, Surf Interfaces* 2023; 17: 363–396.
3. Fahad M. Tribological behavior of AZ91D magnesium alloy composite: effect of hybrid WC–SiO2 nanoparticles. *Ind Lubrication Tribol* 2021; 73: 789–795.
4. Sagar P, Khanna SK, Vignjevic R, et al. Synergistic effect of hybrid reinforcement on magnesium-based composites for enriching mechanical and tribological characteristics. *Proc Inst Mech Eng, Part E: J Process Mech Eng* 2024: 09544089231221683. doi:10.1177/09544089231221683

5. Preethi V, Kavimani V and Gopal PM. Multi-objective optimization of wear and friction behavior of hybrid magnesium-graphene-silicon nitride composite under dry sliding conditions. *Proc Inst of Mech Eng, Part J: J Eng Tribol* 2025: 13506501241313079. doi:10.1177/13506501241313079
6. Surendran KS, Gnanavelbabu A and Rajkumar K. Identification of self-lubricative mode for the ultrasonic treated AA6061-B4C-CNT hybrid composites. *Proc Inst of Mech Eng, Part J: J Eng Tribol* 2023; 237: 784–797.
7. Liu S, Paidar M, Ojo OO, et al. Friction stir processing of hybridized AZ31B magnesium alloy-based composites by adding CeO2 and ZrO2powders: mechanical, wear, and corrosion behaviors. *J Mater Res Technol* 2023; 24: 1949–1972.
8. Arora GS, Gupta A and Saxena KK. Evaluation of mechanical, microstructural, tribological characteristics and cytocompatibility in AZ31 hybrid bio-composite reinforced with tiO2-HAp. *Res Surf Interfaces* 2024; 14: 100174.
9. Anbuchezhiyan G, Mubarak NM, Karri RR, et al. A synergistic effect on enriching the Mg–Al–Zn alloy-based hybrid composite properties. *Sci Rep* 2022; 12: 20053.
10. Mahesha CR, Deshmukh RG, Sunagar P, et al. Experimental analysis on tribological characteristics of AZ60A/Gr/BN magnesium composites. *J Nanomater* 2022; 2022: 2312076.
11. Ammisetti DK and Kruthiventi SS. Experimental investigation of the influence of various wear parameters on the tribological characteristics of AZ91 hybrid composites and their machine learning modeling. *J Tribol* 2024; 146: 051704.
12. Ammisetti DK, Chigilipalli BK, Gaddala B, et al. Experimental investigation and machine learning modeling of tribological characteristics of AZ31/B4C/GNPs hybrid composites. *Crystals (Basel)* 2024; 14: 1007.
13. Deka S, Mozafari F and Mallick A. Microstructural, mechanical, tribological, and corrosion behavior of ultrafine biodegradable Mg/CeO2 nanocomposites: machine learning-based modeling and experiment. *Tribol Int* 2023; 190: 109063.
14. Mahakur VK, Bhowmik S and Patowari PK. Tribo-informatics evaluation of dry sliding friction of silanized jute filler reinforced epoxy composites using machine learning techniques. *Tribol Int* 2023; 183: 108388.
15. Jagadeesh GV and Setti SG. Tribological characterization of ball burnished magnesium alloy by wear-burnishing maps, wear maps and artificial intelligence technique. *Arab J Sci Eng* 2023; 48: 3111–3131.
16. Sheikh KA, Khan MM and Bhat MN. Comparative study of wear behaviour of ZA37 alloy, ZA37/SiC composite, and grey cast iron under lubricated conditions: predictive modeling by machine learning. *Tribol Int* 2025; 207: 110623.
17. Zhu Z, Ning W, Niu X, et al. Machine learning-based research on tensile strength of SiC-reinforced magnesium matrix composites via stir casting. *Acta Metallurgica Sinica (English Letters)* 2024; 37: 453–466.
18. Sheikh KA and Khan MM. Predictive modeling of abrasive wear in in-situ TiC reinforced ZA37 alloy: a machine learning approach. *Tribol Int* 2025; 202: 110291.
19. Beniyel M, Sivapragash M, Vettivel SC, et al. Optimization of tribology parameters of AZ91D magnesium alloy in dry sliding condition using response surface methodology and genetic algorithm. *Bull Polish Acad Sci Tech Sci* 2021; 69: 110291.
20. Abebe SK, Beri H, Sinha DK, et al. Wear behavior of AZ61 matrix hybrid composite fabricated via friction stir consolidation: a combined RSM box–Behnken and genetic algorithm optimization. *J Compos Sci* 2023; 7: 75.
21. Packkirisamy V, Thirugnanasambandam A, Bhowmik A, et al. Synergistic approach to wear rate forecasting in AZ31/5% Yttria stabilized zirconia reinforced composite through response surface methodology-genetic algorithm integration. *Proc Inst of Mech Eng, Part J: J Eng Tribol* 2025; 239: 189–199.
22. T. Satish Kumar, et al. used Response Surface Methodology (RSM) to optimize the wear rate of AZ31/TiC surface composites fabricated by friction stir processing, achieving a 41.3% increase in hardness, a 39.1% rise in tensile strength, and a wear rate prediction error within ±4%, confirming the model's accuracy and the effectiveness of TiC reinforcement.
23. Kumar TS, Raghu R, Priyadharshini GS, et al. A study on microstructural, mechanical properties, and optimization of wear behaviour of friction stir processed AZ31/TiC composites using response surface methodology. *Sci Rep* 2024; 14: 18729.
24. Kumar KC, Kumar BR and Rao NM. Tribological parameters optimization of AZ31-SiC composite using whale optimization algorithm. *J Mater Eng Perform* 2023; 32: 2735–2748.
25. Haldar B, Joardar H, Mondal AK, et al. Machine-learning-driven analysis of wear loss and frictional behavior in magnesium hybrid composites. *Crystals (Basel)* 2025; 15: 452.
26. Zhu G, Du X and Sun D. Machine learning accelerated design of magnesium alloys with high strength and high ductility. *Mater Today Commun* 2025; 44: 111894.
27. Ammisetti DK and Kruthiventi SH. Experimental investigation of the influence of various wear parameters on the tribological characteristics of AZ91 hybrid composites and their machine learning modeling. *J Tribol* 2024; 146: 051704.
28. Gurgenc T, Altay O, Ulas M, et al. Extreme learning machine and support vector regression wear loss predictions for magnesium alloys coated using various spray coating methods. *J Appl Phys* 2020; 127: 185103.
29. Pasha MB, Rao RN, Ismail S, et al. Tribo-informatics approach to predict wear and friction coefficient of Mg/Si3N4 composites using machine learning techniques. *Tribol Int* 2024; 196: 109696.
30. Fathi R, Chen M, Abdallah M, et al. Wear prediction of functionally graded composites using machine learning. *Materials (Basel)* 2024; 17: 4523.
31. Mishra A, Jatti VS and Sefene EM. Exploratory analysis and evolutionary computing coupled machine learning algorithms for modelling the wear characteristics of AZ31 alloy. *Mater Today Commun* 2023; 37: 107507.
32. Ayyanar S, Kaliyamoorthy R, Gnanavelbabu A, et al. Friction and wear properties of AZ91D magnesium composites under varying load and tungsten disulphide solid lubricant. *Ind Lubrication Tribol*. 2025 (ahead-of-print).
33. Narayanasamy P and Selvakumar N. Tensile, compressive and wear behaviour of self-lubricating sintered magnesium based composites. *Trans Nonferrous Met Soc China* 2017; 27: 312–323.
34. Aliasker KT, Gopal PM, Naveen S, et al. Exploring the effects of self-lubricating MoS2 in magnesium metal matrix composite: investigation on wear, corrosion, and mechanical properties. *Colloids Surf, A* 2023; 677: 132362.
35. Yin YL, Yu HL, Wang HM, et al. Tribological behaviors of AZ91D magnesium alloy under the lubrication of oil suspended synthetic magnesium silicate hydroxide nanotubes. *J Magnesium Alloys* 2025; 13: 379–397.
36. Kucukosman R, Sukuroglu EE, Totik Y, et al. Effects of graphene oxide addition on wear behaviour of composite

coatings fabricated by plasma electrolytic oxidation (PEO) on AZ91 magnesium alloy. *J Adhes Sci Technol* 2021; 35: 242–255.
37. Behnamian Y, Serate D, Aghaie E, et al. Tribological behavior of ZK60 magnesium matrix composite reinforced by hybrid MWCNTs/B4C prepared by stir casting method. *Tribol Int* 2022; 165: 107299.
38. Khatkar SK, Verma R, Kant S, et al. Effect of reinforcements on the sliding wear behavior of self-lubricating AZ91D-SiC-gr hybrid composites. *Int J Surf Eng Interdisci Mater Sci (IJSEIMS)* 2022; 10: 1–9.
39. Ling M, Mehrez S, Vignesh RV, et al. Investigation on underwater friction stir processing of AZ-61 magnesium alloy. *Mater Today Commun* 2023; 36: 106885.
40. Zhang Y, Zhang K, Vignesh RV, et al. Achieving superior tribological and mechanical properties of AA5754/ZrO2 +hBN hybrid surface composite by using a new tool in the friction stir processing (FSP). *Tribol Int*. 2025; 210: 110720.
41. Zuo Z, Paidar M, Vignesh RV, et al. Evaluating the influence of vibrational assistance friction stir processing on improving the wear and mechanical properties of hybrid composite AZ31 Mg alloy. *J Mater Res Technol* 2025; 36: 5040–5049.